Fusion enhancement within a collective clusterization approach applied to the isotopic chain of neutron-rich light-mass compound nuclei

Sarbjeet Kaur,[1,2] Navjot Kaur,[2] Rupinder Kaur,[3] BirBikram Singh,[2,*] and S. K. Patra[4,5]

[1]*Department of Physics, Sri Guru Granth Sahib World University, Fatehgarh Sahib 140406, India*
[2]*Department of Physics, Akal University, Talwandi Sabo, Punjab 151302, India*
[3]*Department of Physics, Punjabi University, Patiala 147002, India*
[4]*Homi Bhabha National Institute, Anushakti Nagar, Mumbai, Maharashtra 400094, India*
[5]*Institute of Physics, Sachivalya Marg, Bhubaneswar, Odisha 751005, India*

(Received 13 September 2022; accepted 6 January 2023; published 24 January 2023)

The dynamics of neutron-rich light-mass compound nuclei ^{24,25,26,27}Mg* formed in ^{12,13,14,15}C + ^{12}C fusion reactions, respectively, is explored at different $E_{\rm c.m.}$ values within the dynamical cluster decay model (DCM). DCM is based on the quantum mechanical fragmentation theory, which treats the binary fragmentation of emitting compound nucleus as light particles (LPs), intermediate mass fragments (IMFs), as well as symmetric mass fragments (SMFs), on equal footing, which is not the case with other fission and statistical models. All calculations are made for spherical considerations and angular momenta taken up to the ℓ-critical value for the respective reactions. A fusion enhancement is observed as we go from compound nuclei (CN) having an even number of neutrons (^{24,26}Mg*) to CN with the odd number of neutrons (^{25,27}Mg*). Interestingly, we find that the only parameter of the DCM, the neck-length parameter ΔR related to the barrier lowering, is in linear relation with $\sigma_{\rm Fusion}$ at chosen incident laboratory energy. The fusion enhancement is found to be larger for odd neutron number nuclei, which indicates the influence of unpaired neutrons on fusion cross sections. Within the formalism of DCM, the phenomenon of fusion enhancement finds its base in the process of collective clusterization, which is quite evident from the larger values of summed-up preformation probability for the reactions having odd mass projectiles or forming odd mass CN. The DCM calculated fusion cross sections are in good agreement with the available experimental data for the given reactions.

DOI: 10.1103/PhysRevC.107.014613

I. INTRODUCTION

The dynamics of neutron-rich light-mass compound nuclei ^{24,25,26,27}Mg* formed in ^{12,13,14,15}C + ^{12}C fusion reactions, respectively, are studied within the dynamical cluster decay model (DCM), as we found that these reactions also play a significant role in astrophysical scenarios. After helium burning, a large concentration of ^{12}C in the core of massive stars leads to carbon burning driven by the ^{12}C + ^{12}C fusion reaction. The ^{12}C + ^{12}C fusion reaction is the primary route for the nucleosynthesis of heavier elements and a crucial process in the later phases of stellar evolution and explosions [1,2]. The carbon fusion reaction is also considered to be responsible for igniting stellar explosions such as core-collapse supernovas and x-ray superbursts. X-ray superbursts are a recently observed explosive phenomenon, and are the brightest, most energetic, and rare explosions considered to be triggered by the unstable ^{12}C + ^{12}C fusion in the crust of neutron stars [3].

The exploration of the dynamics and cross sections of these low-energy neutron-rich carbon reactions is one of the most important topics for understanding a number of astrophysical scenarios. But the presence of unpredictable ^{12}C + ^{12}C resonance structures results in large uncertainties in their astrophysical cross sections [4–6]. In comparison to these resonances, other carbon isotope fusion reactions such as ^{12}C + ^{13}C behave more regularly. The resonance structures in low-energy carbon fusion reactions were studied using the correlation to carbon isotope fusion reactions [7–10]. The investigations of fusion for an isotopic chain of neutron-rich nuclei are also important, as the Coulomb potential of the neutron-rich projectile is largely unaffected by adding neutrons. Consequently, it helps to probe the neutron density distribution and provides information about the evolution of density distribution as two nuclei approach and overlap in nuclear fusion [11,12]. This approach resulted in the discovery of the halo nature of ^{11}Li [13].

In view of these experimental observations, we recently investigated the dynamic aspects associated with reactions involving neutron-rich isotopic chains of reactions (^{39,40,41,45,46,47}K + ^{28}Si) [14] within the DCM [14–24]. The result shows that the fusion enhancement is larger for odd neutron number nuclei as compared to adjacent neutron nuclei and indicates the influence of unpaired neutrons on fusion crosssections. That work was for the neutron-rich mid-mass systems ($^{67–69,73–75}$As*); now we have shifted to the lower mass region of $^{12–15}$C + ^{12}C induced $^{24–27}$Mg* CN. The total fusion cross sections of these neutron-rich light-mass carbon

*drbirbikramsingh@gmail.com

isotopes were obtained recently by using the newly developed MUSIC detector [25].

Within DCM, the fusion cross sections σ_{Fusion} of the reactions involving the loosely bound projectiles ^{7}Li, ^{7}Be, and ^{9}Be on different targets leading to the formation of CN in the mass region $A \approx 30$–200 have also been studied by exploring the typical characteristic of the neck-length parameter (ΔR) [20]. It is observed that the empirically fitted ΔR, the only parameter of the DCM, can be fixed uniquely for a particular set of reactions in reference to the available experimental data. Furthermore, this optimized ΔR has been utilized to calculate or predict the σ_{Fusion} of the reactions with the same projectile and the same energy on some stable targets, for which experimental data is not available [14,20].

Moreover, the clustering effects on the reaction dynamics of compound systems ^{24,25}Mg* formed via respective entrance channels ^{12}C + ^{12}C and ^{13}C + ^{12}C were also studied in previous works [23,24]. DCM successfully recognized that the presence of the α-cluster structure in fragments under investigation contributes relatively more towards the yield as compared to fragments without the α cluster. The DCM calculated results are a little better in comparison with the statistical models due to the inclusion of structure effects in the calculations. The clustering effects in other light-mass $N = Z$ (^{20}Ne*, ^{28}Si*, and ^{40}Ca*) and $N \neq Z$ (^{21,22}Ne* and ^{39}K*) composite systems [21], with considerations of quadrupole deformations and compact orientations of nuclei, have also been studied within DCM. This also explores the role of nuclear structure effects, which enters in DCM through preformation probability P_0 of different clusters. In this study, by using ^{12,13,14,15}C projectiles on the same ^{12}C target at the same center-of-mass energies, we will further explore the significance of the neck-length parameter ΔR in the DCM, which simply accounts for the interaction-barrier modification of preformed clusters.

With this motivation in present work, the dynamics of neutron-rich light-mass CN ^{24,25,26,27}Mg* formed in ^{12,13,14,15}C + ^{12}C fusion reactions, respectively, is explored at different $E_{\text{c.m.}}$ values within the DCM. All calculations are made for spherical consideration of nuclei and angular momenta taken up to the ℓ-critical value for the respective reactions. The DCM calculated results have been compared with the available experimental data [25].

In the following section, the methodology followed for the work is given briefly, along with discussions of the presented calculations in the subsequent section, before summarizing the whole work in the last section.

II. THE DYNAMICAL CLUSTER-DECAY MODEL FOR HOT AND ROTATING COMPOUND SYSTEM

The DCM for a hot ($T \neq 0$) and rotating (angular momentum $\ell \neq 0$) compound nucleus (CN) is a reformulation of the preformed cluster model (PCM) of Gupta and collaborators for ground-state ($T = 0$) decays in cluster radioactivity (CR) and related phenomena [15,26–28]. The DCM has been applied successfully to a large number of different reactions belonging to various mass regions from light to superheavy compound systems [14–24]. It involves the two-step process

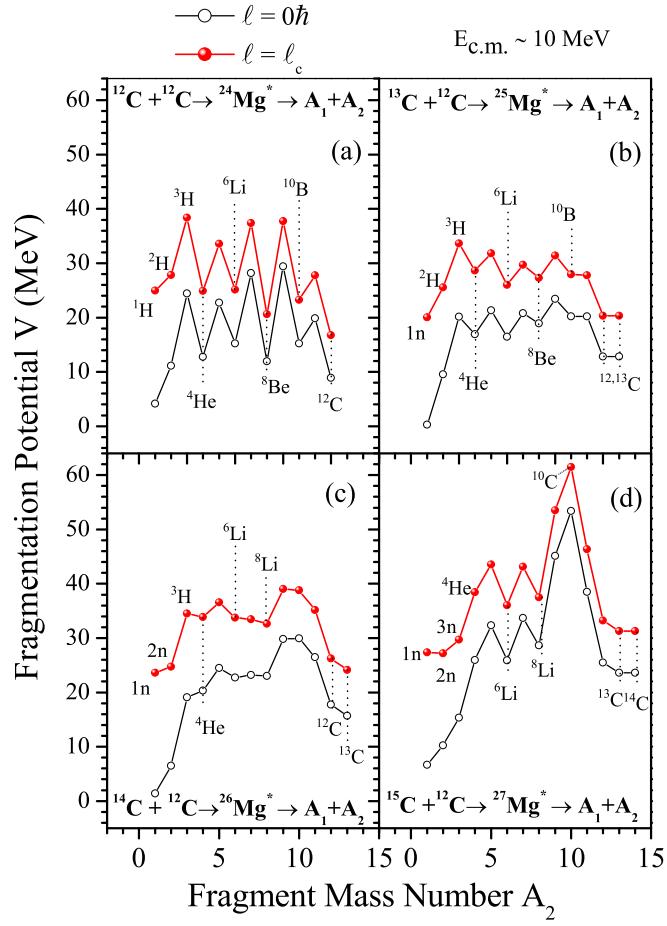

FIG. 1. The fragmentation profile of the CN (a) ^{24}Mg*, (b) ^{25}Mg*, (c) ^{26}Mg*, (d) ^{27}Mg* at $E_{\text{c.m.}} \approx 10$ MeV at $\ell = 0\hbar$ and the respective ℓ_c values.

of cluster preformation followed by the penetration through the interaction barrier, analogous to the α decay where preformation is unity. The structure effects of CN are thus included via the preformation factor. The only parameter of the DCM is the neck-length parameter (ΔR), whose value varies within the range of nuclear proximity (≈2 fm) to fit with the experimental data.

The model, following the quantum mechanical fragmentation theory (QMFT) [29–32], is worked out in terms of the following collective coordinates: The mass asymmetry $\eta_A = \frac{A_1 - A_2}{A_1 + A_2}$ and relative separation coordinate R between two interacting nuclei or two fragments.

In terms of these collective coordinates, using the partial wave analysis, the CN decay or formation cross section in DCM is

$$\sigma = \sum_{\ell=0}^{\ell_c} \sigma_\ell = \frac{\pi}{k^2} \sum_{\ell=0}^{\ell_c} (2\ell + 1) P_0 P, \quad k = \sqrt{\frac{2\mu E_{\text{c.m.}}}{\hbar^2}}. \tag{1}$$

Here, P_0 is the preformation probability, referring to η motion, and P is the penetrability, referring to R motion. μ is the reduced mass and ℓ_c is the critical angular momentum of

colliding nuclei at a given $E_{\rm c.m.}$ is defined as

$$\ell_c = R_a\sqrt{2\mu[E_{\rm c.m.} - V(R_a, \eta_{in}, \ell = 0)]}/\hbar \tag{2}$$

Preformation probabilities P_0 of the fragments are given by the solutions of the stationary Schrödinger equation in η at fixed $R = R_a$,

$$\left\{-\frac{\hbar^2}{2\sqrt{B_{\eta\eta}}}\frac{\partial}{\partial\eta}\frac{1}{\sqrt{B_{\eta\eta}}}\frac{\partial}{\partial\eta} + V_R(\eta, T)\right\}\psi^{\nu}(\eta) = E^{\nu}\psi^{\nu}(\eta), \tag{3}$$

with $\nu = 0, 1, 2, 3, \ldots$ referring to ground-state ($\nu = 0$) and excited-states solutions. The mass parameters $B_{\eta\eta}$ in Eq. (3) are the smooth classical hydrodynamical masses [33].

The preformation probability P_0, presented in Fig. 3, contains the structure information of the CN, which enters via the minimized fragmentation potential shown in Fig. 2 for different CN chosen, and is calculated according to the Strutinsky renormalizing procedure ($B = V_{\rm LDM} + \delta U$), as

$$\begin{aligned} V_R(\eta, T) = &-\sum_{i=1}^{2}[V_{\rm LDM}(A_i, Z_i, T)] \\ &+ \sum_{i=1}^{2}[\delta U_i]\exp\left(-\frac{T^2}{T_0^2}\right) \\ &+ V_P(R, A_i, \beta_{\lambda i}, \theta_i, \Phi, T) \\ &+ V_c(R, Z_i, \beta_{\lambda i}, \theta_i, \Phi, T) \\ &+ V_\ell(R, A_i, \beta_{\lambda i}, \theta_i, \Phi, T). \end{aligned} \tag{4}$$

Here, $V_{\rm LDM}(T)$ is the T-dependent liquid drop energy of Davidson *et al.* [34] and the "empirical" shell corrections δU are from Myers and Swiatecki [35], taken to go to zero exponentially with T. $T_0 = 1.5$ MeV is taken from Jensen and Damgaard [36], which means that the shell correction term becomes nearly zero for $T > 1.5$ MeV. T dependence is also included in nuclear proximity potential V_P, Coulomb potential V_c, and ℓ-dependent potential V_ℓ, for deformed, oriented nuclei. For further details, refer to [17]. It is relevant to mention here that the modified temperature dependence of the pairing energy coefficient $\delta(T)$ is allowed in the $V_{\rm LDM}(T)$ (see Fig. 3 of Ref. [37]). We have highlighted the significance of the modified $\delta(T)$ for ^{12,13}C + ^{12}C induced ^{24,25}Mg* in our previous work [24], hence we will use this modified pairing energy coefficient $\delta(T)$ in our present work.

The penetrability P in Eq. (1) refers to R motion obtained by the Wentzel-Kramers-Brillouin (WKB) approximation, where the scattering potential $V(R)$ is used. For a fixed η, the potential $V(R)$ is defined as the sum of Coulomb, proximity, and angular momentum-dependent potentials, where temperature, deformation, and orientation effects are duly included, i.e.,

$$V(R, \ell, T) = V_c(R, Z_i, T) + V_p(R, A_i, T) + V_\ell(R, A_i, T). \tag{5}$$

The scattering potential calculated by using Eq. (5) for ^{24}Mg $\rightarrow$ ^{23}Na + ^{1}H and $^{25\text{–}27}$Mg* $\rightarrow$ $^{24\text{–}26}$Mg + ^{1}n is shown in Fig. 4. It is clear from Fig. 4 that the excited state decay from the first turning point R_a to the second R_b follows a single

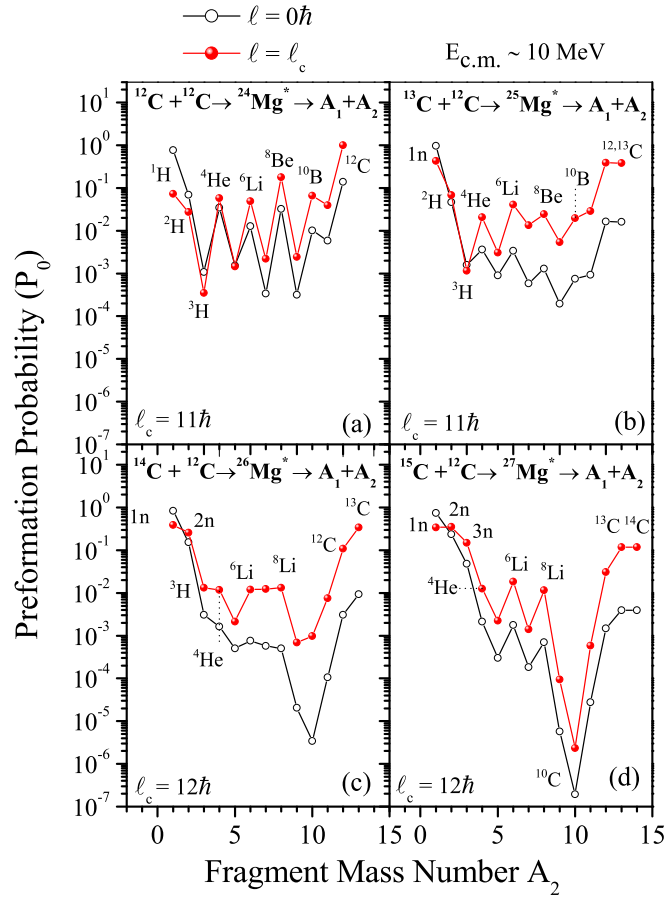

FIG. 2. Same as Fig. 1, but for the preformation probability (P_0).

penetration path. The path of the penetration and the related quantities are also shown in Fig. 4.

The first (inner) turning point R_a is chosen at $R_a = R_t + \Delta R$, where $R_t = R_1 + R_2$ and the outer turning point is taken at R_b to give the Q value of the reaction, i.e., $V(R_b) = Q$. $\Delta R(T)$ is the neck-length parameter that assimilates the neck formation effects between two nuclei, introduced within the extended model of Gupta and collaborators [38–40]. This method of using the neck-length parameter is similar to that used in both the scission-point [41], and saddle-point [42,43] statistical fission models.

The corresponding potential $V(R_a, \ell)$ is related to the top of the barrier $V_B(\ell)$ for each ℓ value by defining their difference $\Delta V_B(\ell)$ as the effective "barrier lowering,"

$$\Delta V_B(\ell) = V(R_a, \ell) - V_B(\ell). \tag{6}$$

Note that, as the barrier is effectively lowered, ΔV_B for each ℓ is defined as a negative quantity, as shown in Fig. 4. Thus, the fitting parameter ΔR controls the "barrier lowering" ΔV_B.

For R motion, using the WKB approximation, the P or the tunneling probability is calculated as

$$P = \exp\left(-\frac{2}{\hbar}\int_{R_a}^{R_b}\{2\mu[V(R, T) - Q_{\rm eff}]\}^{1/2}dR\right), \tag{7}$$

solved analytically [44,45], with R_a and R_b as the first and second turning points. This means that the tunneling begins at

R = R_a and terminates at $R = R_b$ and satisfies the equation

$$V(R_a) = V(R_b) = Q_{\text{eff}}. \tag{8}$$

III. CALCULATIONS AND DISCUSSIONS

In this section, present the calculations for the decay processes of neutron-rich light-mass CN ^{24,25,26,27}Mg* at different center-of-mass energies $E_{\text{c.m.}} \approx 10$ to 14 MeV using the spherical configuration. The fusion cross-sections (σ_{Fusion}) are calculated via fragmentation potential, preformation probability of possible fragments, and their subsequent penetration through scattering potential, and the σ_{Fusion} will be compared with the available experimental data. This section describes the role of the above-mentioned variables in obtaining the σ_{Fusion} and the involved dynamics.

The fragmentation profile as a function of fragment mass number A_2 of the decaying ^{24,25,26,27}Mg* nuclei is shown in Figs. 1(a)–1(d) at angular momentum values $\ell = 0\hbar$ and $\ell = \ell_c$ differentiated by a hollow circle and filled sphere, respectively, at the same $E_{\text{c.m.}} \approx 10$ MeV. It is observed in Fig. 1 that when we move from Fig. 1(a) to 1(d), i.e., from ^{24}Mg* to ^{27}Mg*, respectively, the LPs ($A \leqslant 4$) start becoming more favored or minimized. Note that some LPs change on going from ^{24}Mg* to ^{27}Mg*. The ^{1}H channel of ^{24}Mg* is replaced by $1n$ in the case of ^{25,26,27}Mg*; the ^{2}H channel is present in ^{24,25}Mg* and is replaced by $2n$ as we go to ^{26,27}Mg*; moving to ^{27}Mg*, $3n$ is present in place of ^{3}H. First, LPs compete with symmetric mass fragments (SMFs), mostly with C fragments. The competition between LPs and SMFs decreases going from Fig. 1(a) to 1(d), or LPs start being more favored. This decrease in competition is greater when we move from nuclei having paired neutrons (^{24,26}Mg*) to nuclei having unpaired neutrons (^{25,27}Mg*).

In Fig. 1(a), the LPs ^{1,2,3}H have greater value of fragmentation potential compared to $1n$ and ^{2,3}H in Fig. 1(b). The LP ^{4}He has more fragmentation potential in Fig. 1(b) as compared to Fig. 1(a), i.e., for ^{25}Mg* and ^{24}Mg*, respectively. Hence, as we move from paired ^{24}Mg* to unpaired ^{25}Mg*, the overall fragmentation potential of LPs starts decreasing, i.e., LPs are more favored in the case of unpaired ^{25}Mg*. Continuing from Fig. 1(b) to Fig. 1(c), the LPs $1n$ and ^{4}He are more favored in ^{25}Mg*, and $2n$ and ^{3}H are more favored in ^{26}Mg*. which results in almost the same fragmentation potential of LPs ($A \leqslant 4$) as we move from unpaired ^{25}Mg* to paired ^{26}Mg*. Further moving from Fig. 1(c) to Fig. 1(d), i.e., from paired ^{26}Mg* to unpaired ^{27}Mg*, we observe that LPs $1n$, $2n$, and ^{4}He start having more fragmentation potential. The LP ^{3}H in ^{26}Mg* has more fragmentation potential as compared to $3n$ in ^{27}Mg*, Which results in more favored $3n$ in unpaired ^{27}Mg*. These results are more profound in Fig. 2.

Figures 2(a) to 2(d) present the preformation probability P_0 of the CN $^{24-27}$Mg* at $E_{\text{c.m.}} \approx 10$ MeV at indicated ℓ and ℓ_c values. Here the enhancement in P_0 is observed in nuclei having odd neutrons as compared to even neutron nuclei. When we move from ^{24}Mg* (paired) to ^{25}Mg* (unpaired) the more preformed ^{1}H is replaced by $1n$ having comparatively larger P_0; the rise in P_0 for ^{2,3}H is also observed. Similarly moving from Fig. 2(c) to Fig. 2(d), i.e., ^{26}Mg* (paired) to ^{27}Mg* (unpaired), $1n$, $2n$, and $3n$ fragments start playing a dominant role in fusion. But moving from unpaired ^{25}Mg* to paired ^{26}Mg*, the LPs $1n$ and ^{4}He have higher P_0 in Fig. 2(b), as do the LPs $2n$ and ^{3}H in Fig. 2(c); i.e., the overall increase in the P_0 of LPs is almost the same. In the preformation profile, the $^{12-14}$C fragments also have a higher contribution as compared to LPs, but their fusion yield is low due to their very low penetrability P values, as shown in Fig. 6. Hence the LPs makes the largest contribution to fusion cross section.

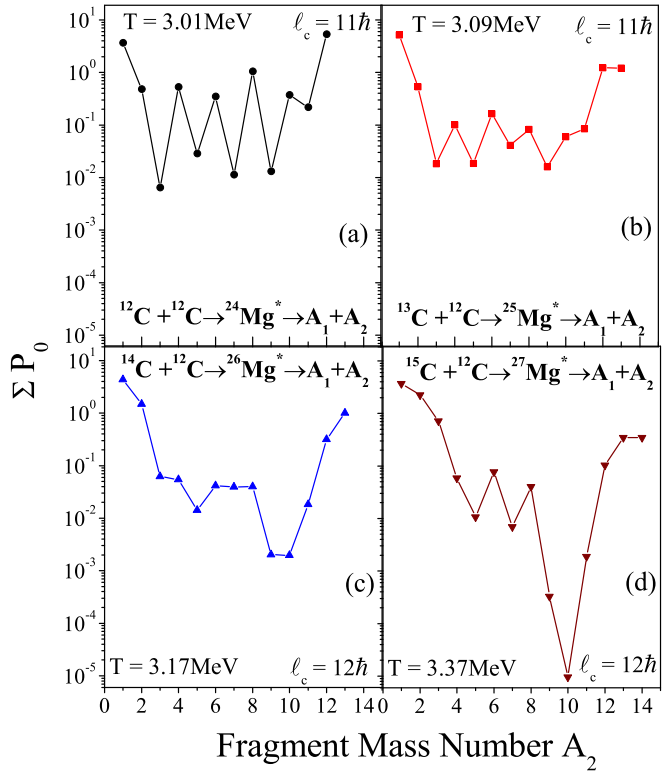

FIG. 3. The variation of ℓ-summed preformation probability ($\sum P_0$) as a function of fragment mass number (A) for the decay of CN (a) ^{24}Mg*, (b) ^{25}Mg*, (c) ^{26}Mg*, (d) ^{27}Mg* at $E_{\text{c.m.}} \approx 10$ MeV

Figures 3(a)–3(d) present ℓ-summed preformation probability ($\sum P_0$) as a function of fragment mass number (A) for CN $^{24-27}$Mg* at $E_{\text{c.m.}} \approx 10$ MeV calculated for indicatedℓ_c values. The P_0 of individual fragments at $\ell = 0$ and $\ell = \ell_c$ values is explored in Fig. 2; here in Fig. 3, the $\sum P_0$ up to $\ell = \ell_c$ is presented. The $\sum P_0$ of LPs $1n$ and ^{2,3}H in ^{25}Mg* is greater compared to ^{24}Mg*, and $\sum P_0$ of only ^{4}He is higher in ^{24}Mg*. That is, we observe an enhancement in the yield of unpaired CN as we move from paired CN. This enhancement is very small as we move to paired CN ^{26}Mg* from unpaired CN ^{25}Mg* due to the almost equal contribution of LPs. The LPs $1n$ and ^{4}He have higher $\sum P_0$ in ^{25}Mg*, but LPs $2n$ and ^{3}H have higher contribution in ^{26}Mg*. Again moving from 3(c) to 3(d), i.e., paired to unpaired CN, there is an enhancement in $\sum P_0$ of LPs in ^{27}Mg* with a major contribution of LPs $1n$, $2n$, $3n$. We also observed a higher contribution of symmetric and near symmetric fragments, which goes on decreasing with increasing mass of CN. The next step is the calculation of the scattering potentials of the preformed fragments. The

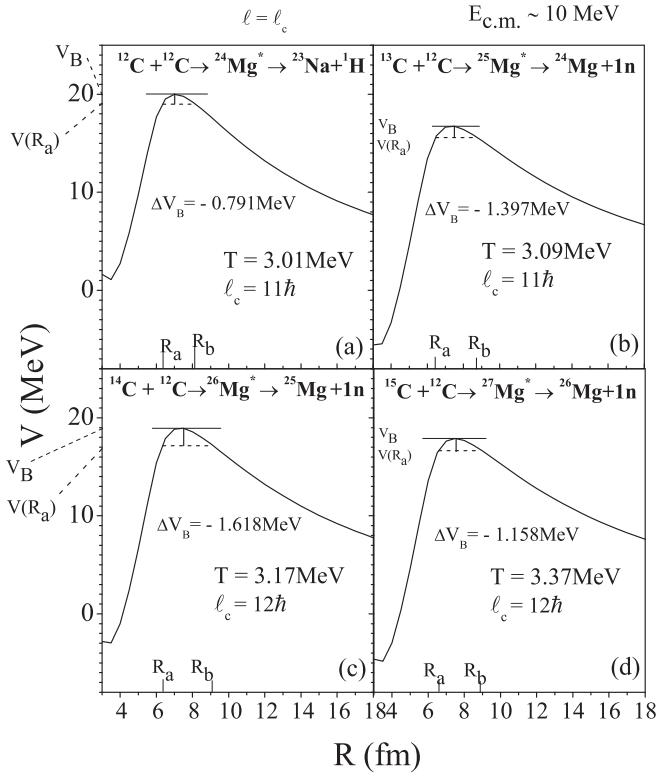

FIG. 4. The scattering potential V for the compound nuclei (a) ^{24}Mg*, (b) ^{25}Mg*, (c) ^{26}Mg*, (d) ^{27}Mg* decaying through one of the probable exit channels at $E_{\text{c.m.}} \approx 10$ MeV at $\ell = \ell_c$ value.

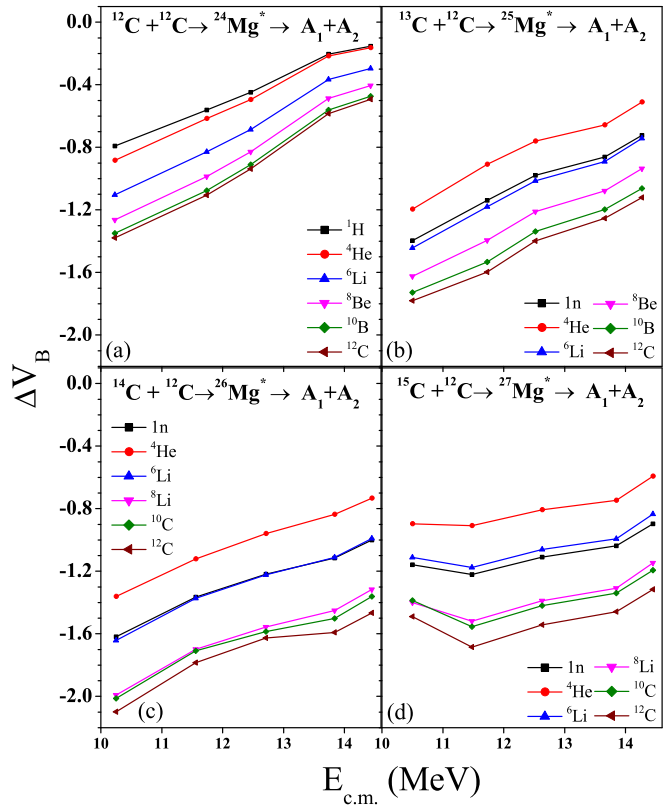

FIG. 5. The barrier lowering ΔV_B as a function of $E_{\text{c.m.}}$ for the case of ℓ_c for the compound nuclei (a) ^{24}Mg*, (b) ^{25}Mg*, (c) ^{26}Mg*, (d) ^{27}Mg*.

scattering potentials for all the compound nuclei, decaying through one probable exit channel at extreme ℓ value, are shown in Figs. 4(a)–4(d). R_a and R_b correspond to the first and second turning points for the respective exit channel, which, in detail, is already discussed in the methodology section. Figs. 5(a) and 5(b) show ΔV_B as a function of fragment mass number. The barrier lowering for different exit channels determines the penetration probability (P) of the respective fragments and is quite evident from $\sum P$ of fragments in Figs. 6(a)–6(d), where it can be observed that the inverse trend of ΔV_B is followed by $\sum P$. As for the LPs, ΔV_B is less, so its $\sum P$ is greater, as presented in the following figure. The barrier lowering for the symmetric and near symmetric exit channels is relatively more, resulting in very small values of penetrability, quite evident from Fig. 6.

Figures 6(a)–6(d) present ℓ-summed penetrability ($\sum P$) as a function of fragment mass number (A) for CN $^{24-27}$Mg* at $E_{\text{c.m.}} \approx 10$ MeV calculated for indicated ℓ_c values. Here, the $\sum P$ is large mainly for the LPs, and consequently with the large $\sum P_0$ they contributed more toward the fusion yield. In Figs. 2 and 3, the $^{12-14}$C fragments also have higher preformation probabilities, but their penetrability through the barrier is minimum, as shown in Fig. 6. Hence the major contribution in σ_{Fusion} is mainly due to the contributions of LPs, as observed experimentally. By comparing the results of Fig. 6(a)–6(d), i.e., on moving from paired CN to unpaired CN and unpaired CN to paired CN, no specific trends are observed. Hence we

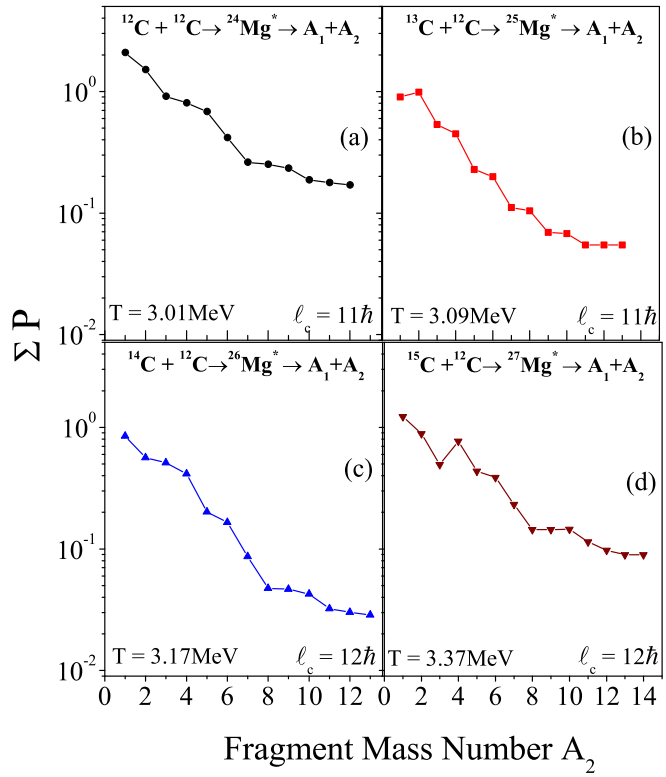

FIG. 6. Same as Fig. 3 but for ℓ-summed penetrability ($\sum P$).

TABLE I. The DCM calculated fusion cross sections (σ_{Fusion}) for the compound nuclei $^{24-27}$Mg* at seven different energies and their comparison with the experimental data of Carnelli *et al.* [25] and previous experimental data [5,7].

CN	$E_{\text{c.m.}}$ (MeV)	E^*_{CN} (MeV)	T (MeV)	ℓ_c ($\hbar$)	ΔR (fm)	σ_{Fusion} DCM (mb)	σ_{Fusion} Expt. [25] (mb)	σ_{Fusion} Expt. [5,7] (mb)
				$E_{\text{c.m.}} \approx 10.37$ MeV				
^{24}Mg*	10.23	24.164	3.01	11	1.863	556.89	556.71 ± 51.4	580 ± 19.33
^{25}Mg*	10.50	26.818	3.09	11	1.817	737.03	738.14 ± 41.23	734 ± 12
^{26}Mg*	10.25	29.484	3.17	12	1.738	744.39	746.39 ± 63.6	
^{27}Mg*	10.50	34.959	3.37	12	1.926	1032.34	1031.58 ± 143.5	
				$E_{\text{c.m.}} \approx 11.63$ MeV				
^{24}Mg*	11.74	25.673	3.097	12	1.881	614.27	614.43 ± 53.7	600 ± 16.28
^{25}Mg*	11.73	28.046	3.160	13	1.746	809.47	808.25 ± 47.8	
^{26}Mg*	11.56	30.794	3.236	12	1.810	839.97	841.24 ± 74.5	
^{27}Mg*	11.48	36.299	3.431	14	1.773	1023.47	1020.24 ± 133.4	
				$E_{\text{c.m.}} \approx 12.58$ MeV				
^{24}Mg*	12.46	26.394	3.13	12	1.937	691.93	692.78 ± 55.7	710 ± 20.34
^{25}Mg*	12.52	28.836	3.20	13	1.798	891.17	890.7 ± 43.4	843 ± 18
^{26}Mg*	12.71	31.940	3.29	13	1.785	950.08	952.58 ± 88.4	
^{27}Mg*	12.63	37.089	3.47	14	1.810	1054.89	1054.25 ± 139.3	
				$E_{\text{c.m.}} \approx 13.77$ MeV				
^{24}Mg*	13.74	27.67	3.208	13	2.002	773.51	775 ± 57.73	760 ± 21.36
^{25}Mg*	13.66	29.98	3.261	13	1.843	920.62	919.58 ± 60.1	886 ± 19
^{26}Mg*	13.84	33.07	3.348	14	1.750	957.61	960.83 ± 81.8	
^{27}Mg*	13.85	38.31	3.521	14	1.838	1056.05	1054.25 ± 133.5	
				$E_{\text{c.m.}} \approx 14.4$ MeV				
^{24}Mg*	14.43	28.364	3.246	13	2.048	816.26	816.50 ± 57.73	860 ± 21.36
^{25}Mg*	14.27	30.588	3.293	14	1.816	891.70	890.72 ± 48.42	887 ± 16
^{26}Mg*	14.45	30.684	3.377	14	1.787	1017.56	1018.56 ± 82.45	
^{27}Mg*	14.45	38.907	3.547	15	1.815	1152.07	1150.61 ± 138.3	

can conclude that no structure information is present in the ℓ-summed penetrability.

The DCM calculated fusion cross sections (σ_{Fusion}) for the compound nuclei $^{24-27}$Mg* at five different energies, and their comparison with the available experimental data [25] and with more reliable experimental data with much smaller error bars [5,7], are given in Table I. Experimental data of Sperr *et al.* [5] gave σ_{Fusion} for ^{12}C + ^{12}C induced ^{24}Mg* and those of Kovar *et al.* [7] gave values for ^{13}C + ^{12}C induced ^{25}Mg*. The σ_{Fusion} are in good agreement with experimental data [25] and almost in the error bars of the previous data of [5,7] except for four data points, maybe due to the difference in $E_{\text{c.m.}}$ values. This is also presented graphically in Fig. 7. In Fig. 7, hollow squares present DCM calculated σ_{Fusion}. The filled up-triangle, filled down-triangle, and filled circle present experimentally available σ_{Fusion}, for ^{24}Mg* [7], ^{25}Mg* [5], and $^{24-27}$Mg* [25], respectively. Results show a very good agreement of the DCM calculated σ_{Fusion} with available experimental data [25]. Figure 7 clearly elaborates the phenomenon of fusion enhancement, as we see that the cross sections of the ^{13}C + ^{12}C reaction forming compound nucleus ^{25}Mg* are larger than those of ^{12}C + ^{12}C induced reactions forming compound nucleus ^{24}Mg*, and in comparison to the reaction ^{14}C + ^{12}C yielding compound nucleus ^{26}Mg*. Furthermore, the compound nucleus ^{27}Mg* formed

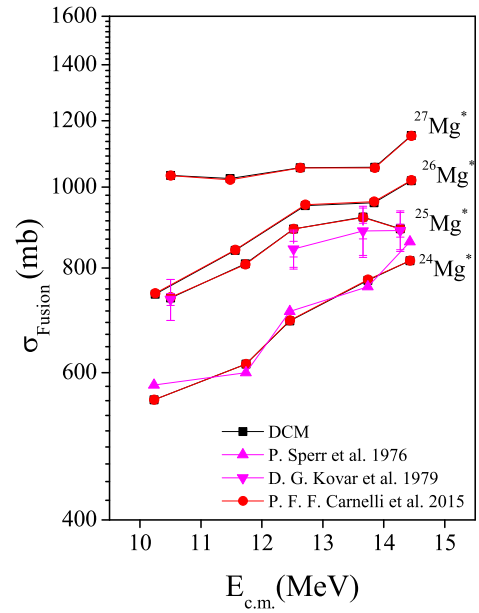

FIG. 7. The variation of fusion cross section σ_{Fusion} with the mass of compound nuclei at comparable center-of-mass energy $E_{\text{c.m.}}$ within DCM and compared with available experimental data.

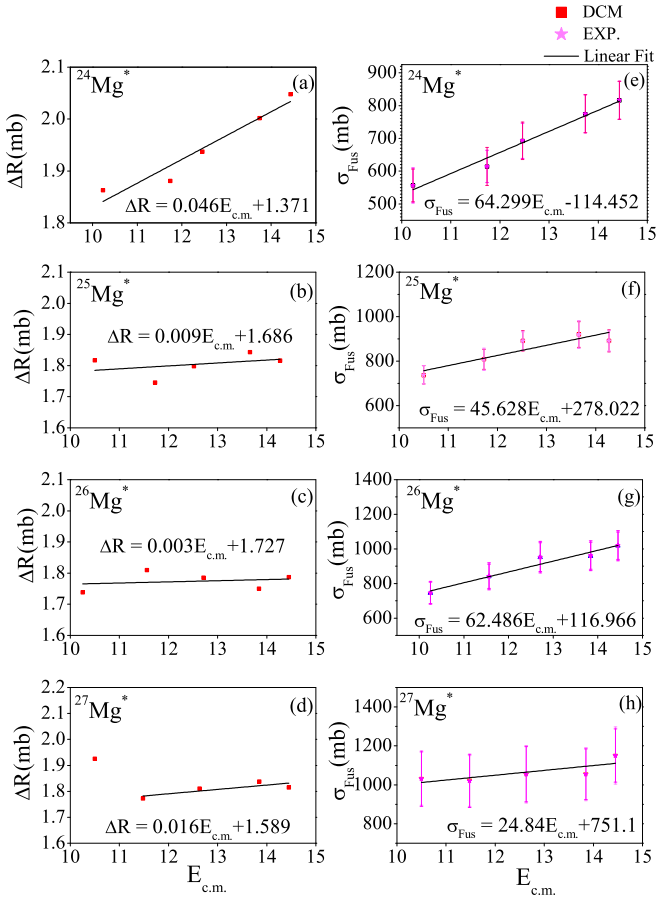

FIG. 8. The linear variation in neck length parameter ΔR (fm) and σ_{Fusion} with $E_{\text{c.m.}}$ (MeV).

in the reaction $^{15}\text{C} + ^{12}\text{C}$ has further fusion enhancement, in comparison to compound nucleus $^{26}\text{Mg}^*$ formed in the reaction $^{14}\text{C} + ^{12}\text{C}$. It is important to note that this observation is consistent with $\sum P_0$ enhancement within the collective clusterization approach of DCM. This phenomenon of fusion enhancement comes naturally within this dynamical expression of low energy heavy ion reactions forming light-mass composite systems.

It must be mentioned here that to calculate these σ_{Fusion} the only parameter of the DCM is the empirically fitted neck length parameter (ΔR). To further explore the trend of empirically fitted neck length parameter (ΔR). The variation in ΔR (fm) with $E_{\text{c.m.}}$ (MeV) is shown in Figs. 8(a)–8(d), and its relation with σ_{Fusion} is shown in Figs. 8(e)–8(h). Note that the value of ΔR varies linearly with $E_{\text{c.m.}}$, which is also true for σ_{Fusion}.

IV. SUMMARY AND CONCLUSIONS

The dynamics of neutron-rich light-mass compound nuclei $^{24,25,26,27}\text{Mg}^*$ induced by $^{12,13,14,15}\text{C} + ^{12}\text{C}$ reactions, respectively, have been explored through fragmentation potential, preformation probability, penetration probability, etc., in order to see the effect of neutron excess in CN. First, LPs compete with SMFs, but by adding more neutrons this competition decreases, and LPs start being more favored. The fragmentation potential surface and preformation probability depict that as we move from nuclei having paired neutrons ($^{24,26}\text{Mg}^*$) to nuclei having unpaired neutrons ($^{25,27}\text{Mg}^*$), LPs start dominating. The IMFs and SMFs have contributions in fragmentation and preformation probability profiles, but their higher barrier-lowering values result in minimum penetrability through the barrier, hence very small contribution in σ_{Fusion}, as observed experimentally. We can also conclude that no structure information is present in $\sum P$.

The significant observation in the present work is that the fusion enhancement is observed in nuclei having odd neutrons ($^{25,27}\text{Mg}^*$) as compared to even-neutron ($^{24,26}\text{Mg}^*$) nuclei. Interestingly, we also find that the only parameter of the DCM, the neck-length parameter ΔR (fm) related to the barrier lowering, varies linearly as σ_{Fusion} for different reactions, with respect to center-of-mass energies $E_{\text{c.m.}}$. The motivation behind the future work is to reduce the degree of freedom for fixing the value of ΔR. The calculated σ_{Fusion} are in good agreement with the available experimental data [25]. The present carbon fusion reactions are responsible for igniting stellar explosions and are one of the most important topics for understanding a number of astrophysical scenarios. The good agreement of DCM calculated σ_{Fusion} with experimental data [25] will motivate future exploration with other neutron-rich beams.

[1] G. Wallerstein, I. Iben Jr., P. Parker, A. M. Boesgaard, G. M. Hale, A. E. Champagne, C. A. Barnes, F. Käppeler, V. V. Smith, R. D. Hoffman, F. X. Timmes, C. Sneden, R. N. Boyd, B. S. Meyer, and D. L. Lambert, Rev. Mod. Phys. **69**, 995 (1997).
[2] M. Pignatari, R. Hirschi, M. Wiescher, R. Gallino, M. Bennett, M. Beard, C. Fryer, F. Herwig, G. Rockefeller, and F. X. Timmes, Astrophys. J. **762**, 31 (2013).
[3] A. Cumming and L. Bildsten, Astrophys. J. **559**, L127 (2001).
[4] E. Almqvist, D. A. Bromley, and J. A. Kuehner, Phys. Rev. Lett. **4**, 515 (1960).
[5] P. Sperr, T. H. Braid, Y. Eisen, D. G. Kovar, F. W. Prosser, Jr., J. P. Schiffer, S. L. Tabor, and S. Vigdor, Phys. Rev. Lett. **37**, 321 (1976).
[6] B. Bucher, X. Fang, X. D. Tang, W. P. Tan, S. Almaraz-Calderon, A. Alongi, A. D. Ayangeakaa, M. Beard, A. Best, J. Browne, C. Cahillane, M. Couder, E. Dahlstrom, P. Davies, R. deBoer, A. Kontos, L. Lamm, A. Long, W. Lu, S. Lyons, C. Ma *et al.*, EPJ Web Conf. **93**, 03009 (2015).
[7] D. G. Kovar, D. F. Geesaman, T. H. Braid, Y. Eisen, W. Henning, T. R. Ophel, M. Paul, K. E. Rehm, S. J. Sanders, P. Sperr, J. P. Schiffer, S. L. Tabor, S. Vigdor, B. Zeidman, and F. W. Prosser, Jr., Phys. Rev. C **20**, 1305 (1979).
[8] B. Heusch, C. Beck, J. P. Coffin, R. M. Freeman, A. Gallmann, F. Haas, F. Rami, P. Wagner, and D. E. Alburger, Phys. Rev. C **23**, 1527 (1981).

[9] X. Tang, X. Fang, B. Bucher, H. Esbensen, C. L. Jiang, K. E. Rehm, and C. J. Lin, EPJ Web Conf. **17**, 16016 (2011).
[10] C. Beck, A. M. Mukhamedzhanov, and X. Tang, Eur. Phys. J. A **56**, 87 (2020).
[11] R. T. deSouza, V. Singh, S. Hudan, Z. Lin, and C. J. Horowitz, Phys. Lett. B **814**, 136115 (2021).
[12] V. Singh, J. Vadas, T. K. Steinbach, B. B. Wiggins, S. Hudan, R. T. deSouza, Z. Lin, C. J. Horowitz, L. T. Baby, S. A. Kuvin, V. Tripathi, I. Wiedenhöver, and A. S. Umar, Phys. Lett. B **765**, 99 (2017).
[13] I. Tanihata, H. Hamagaki, O. Hashimoto, Y. Shida, N. Yoshikawa, K. Sugimoto, O. Yamakawa, T. Kobayashi, and N. Takahashi, Phys. Rev. Lett. **55**, 2676 (1985).
[14] R. Kaur, M. Kaur, V. Singh, S. Kaur, B. B. Singh, and B. S. Sandhu, Phys. Rev. C **98**, 064612 (2018).
[15] R. K. Gupta and W. Greiner, Int. J. Mod. Phys. E **03**, 335 (1994).
[16] R. K. Gupta, R. Kumar, N. K. Dhiman, M. Balasubramaniam, W. Scheid, and C. Beck, Phys. Rev. C **68**, 014610 (2003).
[17] R. K. Gupta, M. Balasubramaniam, R. Kumar, D. Singh, C. Beck, and W. Greiner, Phys. Rev. C **71**, 014601 (2005).
[18] B. B. Singh, M. K. Sharma, and R. K. Gupta, Phys. Rev. C **77**, 054613 (2008).
[19] B. B. Singh, M. Kaur, M. K. Sharma, and R. K. Gupta, EPJ Web Conf. **86**, 00049 (2015).
[20] M. Kaur, B. B. Singh, M. K. Sharma, and R. K. Gupta, Phys. Rev. C **92**, 024623 (2015).
[21] M. Kaur, B. B. Singh, S. K. Patra, and R. K. Gupta, Phys. Rev. C **95**, 014611 (2017).
[22] M. Kaur, B. B. Singh, S. Kaur, and R. K. Gupta, Phys. Rev. C **99**, 014614 (2019).
[23] R. Kaur, S. Kaur, B. B. Singh, B. S. Sandhu, and S. K. Patra, Phys. Rev. C **101**, 034614 (2020).
[24] S. Kaur, R. Kaur, B. B. Singh, and S. K. Patra, Nucl. Phys. A **1018**, 122361 (2022).
[25] P. F. F. Carnelli, S. Almaraz-Calderon, K. E. Rehm, M. Albers, M. Alcorta, P. F. Bertone, B. Digiovine, H. Esbensen, J. O. F. Niello, D. Henderson, C. L. Jiang, J. Lai, S. T. Marley, O. Nusair, T. Palchan-Hazan, R. C. Pardo, M. Paul, and C. Ugalde, Phys. Rev. Lett. **112**, 192701 (2014); Nucl. Instrum. Methods Phys. Res., Sect. A **799**, 197 (2015).
[26] R. K. Gupta, W. Scheid, and W. Greiner, J. Phys. G: Nucl. Part. Phys. **17**, 1731 (1991).
[27] S. Kumar and R. K. Gupta, Phys. Rev. C **49**, 1922 (1994).
[28] S. K. Arun, R. K. Gupta, B. B. Singh, S. Kanwar, and M. K. Sharma, Phys. Rev. C **79**, 064616 (2009).
[29] J. Maruhn and W. Greiner, Phys. Rev. Lett. **32**, 548 (1974).
[30] R. K. Gupta, Theory of Charge Dispersion in Nuclear Fission, Phys. Rev. Lett. **35**, 353 (1975).
[31] A. Sandulescu, R. K. Gupta, W. Scheid, and W. Greiner, Phys. Lett. B **60**, 225 (1976).
[32] R. K. Gupta, A. Sandulescu, and W. Greiner, Phys. Lett. B **67**, 257 (1977).
[33] H. Kröger and W. Scheid, J. Phys. G **6**, L85 (1980).
[34] N. J. Davidson, S. S. Hsiao, J. Markram, H. G. Miller, and Y. Tzeng, Nucl. Phys. A **570**, 61 (1994).
[35] W. Myers and W. J. Swiatecki, Nucl. Phys. **81**, 1 (1966).
[36] A. S. Jensen and J. Damgaard, Nucl. Phys. A **203**, 578 (1973).
[37] M. Bansal, R. Kumar, and R. K. Gupta, J. Phys.: Conf. Ser. **321**, 012046 (2011).
[38] H. S. Khosla, S. S. Malik, and R. K. Gupta, Nucl. Phys. A **513**, 115 (1990).
[39] S. Kumar and R. K. Gupta, Phys. Rev. C **55**, 218 (1997).
[40] R. K. Gupta, S. Kumar, and W. Scheid, Int. J. Mod. Phys. E **06**, 259 (1997).
[41] T. Matsuse, C. Beck, R. Nouicer, and D. Mahboub, Phys. Rev. C **55**, 1380 (1997).
[42] S. J. Sanders, Phys. Rev. C **44**, 2676 (1991).
[43] S. J. Sanders, D. G. Kovar, B. B. Back, C. Beck, D. J. Henderson, R. V. F. Janssens, T. F. Wang, and B. D. Wilkins, Phys. Rev. C **40**, 2091 (1989).
[44] R. K. Gupta, in *Proceedings of the 5th International Conference on Nuclear Reaction Mechanisms, Varenna, Italy*, edited by Gadioli E (Ricerca Scintifica Educazione Permanente, Milan, 1988), p. 416.
[45] S. S. Malik and R. K. Gupta, Phys. Rev. C **39**, 1992 (1989).